demethylation provide protection against variations that may be encountered in the worm's natural environment. These roles in ensuring the robustness of cell conversion in stressful circumstances may underlie invariant Td under normal conditions. Last, our in vivo results suggest that Set1 and *jmjd-3.1* perform highly conserved roles across phyla and cell types to reinforce TF-driven changes in identity. Indeed, modulation of H3K4 and H3K27 methylation state has been shown to regulate somatic reprogramming (*21–23*). Specifically, the core Set1 subunit, Wdr5, was recently shown to interact with and potentiate Oct4's roles in the initial phases of mammalian induced pluripotent stem (iPS) cell induction (*22*). Furthermore, Jmjd3 was found to specifically inhibit the initial stages of iPS reprogramming (*23*), drawing a distinct parallel to its disruption of the initial stages of Td we observed.

REFERENCES AND NOTES

1. C. Jopling, S. Boue, J. C. Izpisua Belmonte, *Nat. Rev. Mol. Cell Biol.* **12**, 79–89 (2011).
2. E. M. Tanaka, P. W. Reddien, *Dev. Cell* **21**, 172–185 (2011).
3. S. Jarriault, Y. Schwab, I. Greenwald, *Proc. Natl. Acad. Sci. U.S.A.* **105**, 3790–3795 (2008).
4. S. Zuryn, S. Le Gras, K. Jamet, S. Jarriault, *Genetics* **186**, 427–430 (2010).
5. K. Agger *et al.*, *Nature* **449**, 731–734 (2007).
6. F. De Santa *et al.*, *Cell* **130**, 1083–1094 (2007).
7. O. Karakuzu, D. P. Wang, S. Cameron, *Development* **136**, 943–953 (2009).
8. N. J. Francis, R. E. Kingston, C. L. Woodcock, *Science* **306**, 1574–1577 (2004).
9. A. Shilatifard, *Annu. Rev. Biochem.* **81**, 65–95 (2012).
10. J. P. Richard *et al.*, *Development* **138**, 1483–1492 (2011).
11. J. Liang *et al.*, *Nat. Cell Biol.* **10**, 731–739 (2008).
12. K. Kagias, A. Ahier, N. Fischer, S. Jarriault, *Proc. Natl. Acad. Sci. U.S.A.* **109**, 6596–6601 (2012).
13. I. Chambers, S. R. Tomlinson, *Development* **136**, 2311–2322 (2009).
14. P. Kratsios, A. Stolfi, M. Levine, O. Hobert, *Nat. Neurosci.* **15**, 205–214 (2012).
15. I. Issaeva *et al.*, *Mol. Cell. Biol.* **27**, 1889–1903 (2007).
16. Y. W. Cho *et al.*, *J. Biol. Chem.* **282**, 20395–20406 (2007).
17. S. A. Miller, A. C. Huang, M. M. Miazgowicz, M. M. Brassil, A. S. Weinmann, *Genes Dev.* **22**, 2980–2993 (2008).
18. B. E. Bernstein *et al.*, *Cell* **125**, 315–326 (2006).
19. P. Voigt, W. W. Tee, D. Reinberg, *Genes Dev.* **27**, 1318–1338 (2013).
20. P. Voigt *et al.*, *Cell* **151**, 181–193 (2012).
21. A. A. Mansour *et al.*, *Nature* **488**, 409–413 (2012).
22. Y. S. Ang *et al.*, *Cell* **145**, 183–197 (2011).
23. W. Zhao *et al.*, *Cell* **152**, 1037–1050 (2013).

SUPPLEMENTARY MATERIALS

www.sciencemag.org/content/345/6198/826/suppl/DC1
Materials and Methods
Figs. S1 to S16
Table S1
References (*24–42*)

12 May 2014; accepted 17 July 2014
10.1126/science.1255885

Programmable on-chip DNA compartments as artificial cells

Eyal Karzbrun,[1]* Alexandra M. Tayar,[1]* Vincent Noireaux,[2] Roy H. Bar-Ziv[1]†

The assembly of artificial cells capable of executing synthetic DNA programs has been an important goal for basic research and biotechnology. We assembled two-dimensional DNA compartments fabricated in silicon as artificial cells capable of metabolism, programmable protein synthesis, and communication. Metabolism is maintained by continuous diffusion of nutrients and products through a thin capillary, connecting protein synthesis in the DNA compartment with the environment. We programmed protein expression cycles, autoregulated protein levels, and a signaling expression gradient, equivalent to a morphogen, in an array of interconnected compartments at the scale of an embryo. Gene expression in the DNA compartment reveals a rich, dynamic system that is controlled by geometry, offering a means for studying biological networks outside a living cell.

In the past decade, cell-free gene expression reactions have been used to design synthetic biological systems, including droplets for molecular evolution (*1*), a vesicle bioreactor toward an artificial cell (*2*), regulatory (*3–6*) and morphogenetic-like genetic circuits (*7*), as well as assembly of protein complexes (*8–10*). Thus far, the lack of efficient protein turnover has prevented the emergence of expression dynamic patterns, such as oscillations, in a continuous expression bioreactor or vesicle (*2, 11*). Microfluidic chips containing switching valves and addressable fluidic chambers (*12, 13*) have succeeded in implementing steady-state and dynamic protein synthesis reactions (*14*). However, micrometer-scale positional information encoded in diffusive concentration gradients of proteins and mRNA, as in a morphogenetic scenario (*15*), is washed away in flow-driven expression compartments. Here, we present a solid-state biochip approach for the assembly of an artificial cell, which enables protein turnover, materials exchange with the environment, a capacity to encode and express genes at high surface density within a controlled geometry, and the ability to maintain micrometer-scale positional information in diffusive molecular gradients.

Dense phases of end-attached, linear double-stranded DNA templates (DNA brushes) were assembled by chemical photolithography (*16, 17*) on the surface of circular compartments carved in silicon with radius $R = 50$ μm and depth $h = 1$ to 3 μm (Fig. 1, A and B, and figs. S1 to S3). The DNA compartments were connected to a 30-μm-deep flow channel through thin capillaries of width $W = 20$ μm and length $L = 50$ to 300 μm. The device was sealed, and *Escherichia coli* cell extract (*18, 19*) was continuously flown in the main channel. Reaction components were transported by diffusion into the DNA compart-

ment because of the high resistance to flow through the capillary (fig. S4). Proteins were synthesized in the DNA compartment and diffused out to the flow channel through the capillary. A linear protein concentration gradient formed along the capillary, decaying from a maximal value in the DNA compartment, where its distribution was homogenous, down to zero at the channel junction (Fig. 1C). The protein linear gradient persisted throughout the duration of expression, which reached a steady-state concentration (fig. S5). The dilution through the capillary leads to an emergent effective protein lifetime, $\tau = \frac{\pi R^2}{WD}L$, that is obtained by solving the diffusion equation in the compartment geometry, where D is the protein diffusion constant (supplementary materials).

The effective protein lifetime enabled us to observe gene expression dynamics, including steady states (Fig. 1D) and oscillations (Fig. 1E). Figure 1D shows expression of green fluorescent protein (GFP) through a positive feedback gene construct, which is self-activated by the AraC protein dimer in the presence of arabinose (*20*) (fig. S6). The kinetics was characterized by a sharp onset after a 2-hour delay and reached a steady-state level for over 8 hours. To implement an oscillatory gene expression dynamics, we used an activator-repressor network with sigma factor σ^{28} for activation and the lambda phage cI repressor (fig. S6 and tables S1 to S3). The network exhibited emergent oscillations for many hours with a period of ~2.5 hours (Fig. 1E). Furthermore, the high concentration of regulatory proteins near the DNA brush enabled direct imaging of transcription regulation. We imaged repression of transcription by using a negative-feedback construct that codes for a fusion of a Cro repressor dimer and GFP, expressed under a Cro-regulated promoter (fig. S6). The synthesized fusion protein bound the repressor site adjacent to the promoter, thereby localized the GFP signal to the DNA brush (Fig. 1F) and led to a reduced self-regulated expression levels in steady state.

[1]Department of Materials and Interfaces, Weizmann Institute of Science, Rehovot 76100, Israel. [2]Department of Physics, University of Minnesota, Minneapolis, MN 55455, USA.
*These authors contributed equally to this work. †Corresponding author. E-mail: roy.bar-ziv@weizmann.ac.il

In order to investigate the effect of compartment geometry on the reaction-diffusion dynamics, we fabricated a device with varying capillary length and integrated up to 80 compartments on the chip. First, we studied three single-gene constructs as a function of the capillary length: unregulated, positive-feedback, and a negative-feedback construct (Fig. 2, A to C, and fig. S6). GFP appeared in the compartments in hierarchical

Fig. 1. Two-dimensional DNA compartments and emergent gene network dynamics. (**A**) DNA brushes patterned (red squares) in circular compartments ($h \approx 2 \mu m$), carved in silicon, and connected through a diffusive capillary to a channel flowing a cell-free expression reaction. (**B**) Overlay of expressed GFP in the compartment and end-labeled DNA brush images. (**C**) GFP intensity profile in arbitrary units (AU) of an unregulated construct along the capillary after 4 hours of expression. (**D**) Steady-state dynamics of a positive-feedback construct reported by GFP. (**E**) Emergent oscillation of an activator-repressor network. (**F**) Repressor-GFP fusion binding its own promoter during expression of a self-repressed DNA construct. Scale bar indicates 100 μm. GFP intensity was taken from single reactors and averaged over the compartment area with error bars the size of data points.
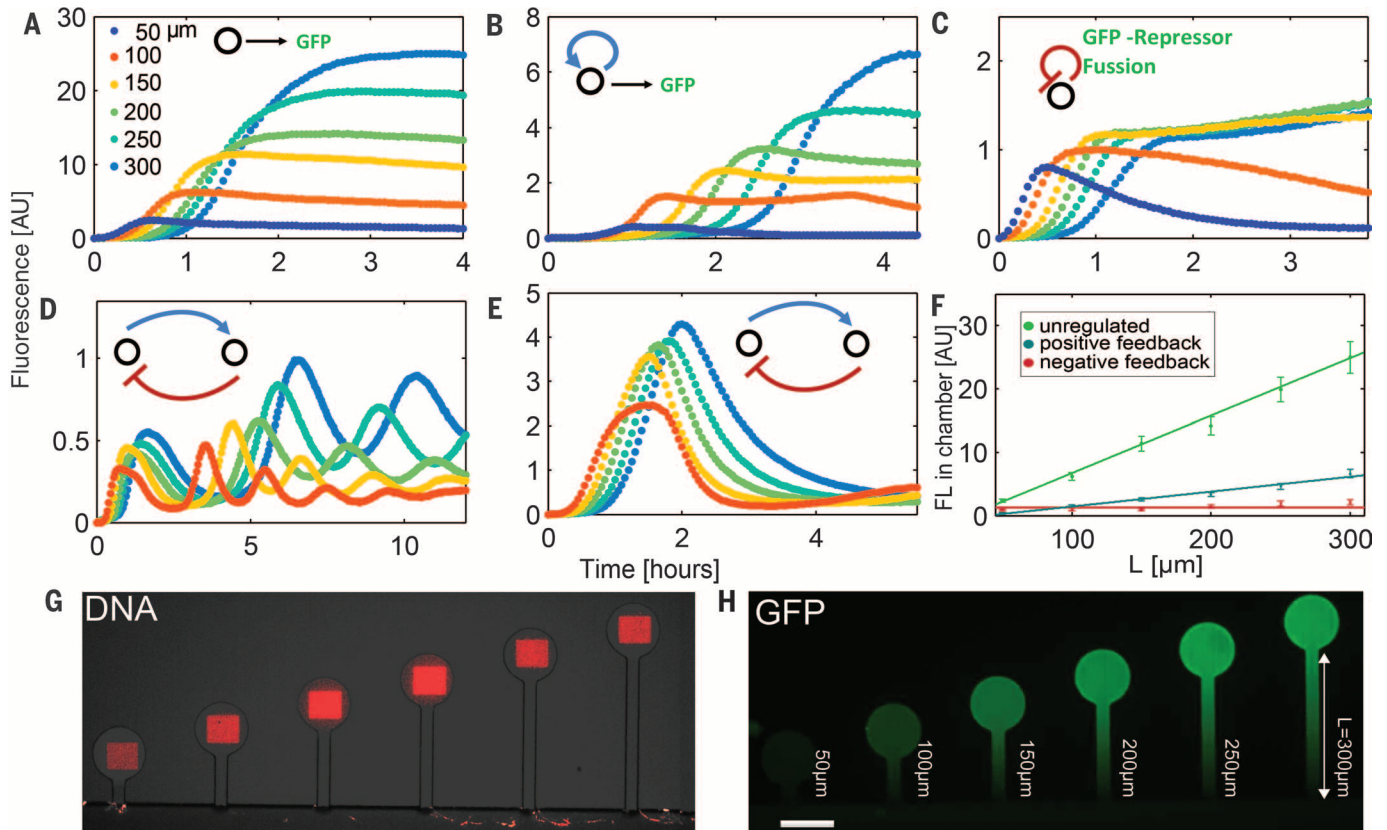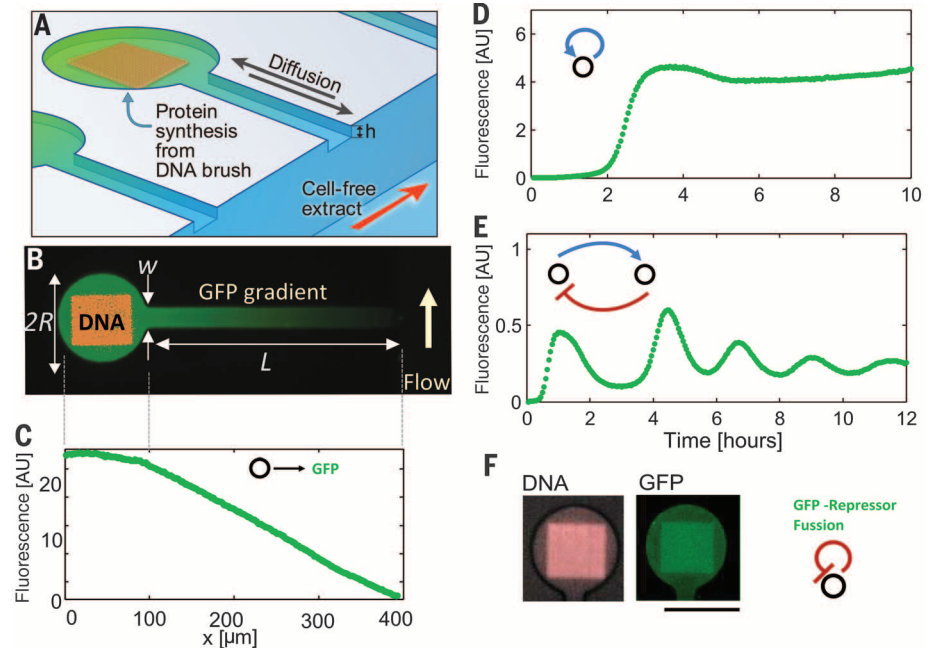

Fig. 2. Gene network dynamics regulated by geometry. Expression dynamics of GFP in the DNA compartment with $L = 50$ to 300 μm as denoted and for five different constructs: (**A**) unregulated, (**B**) positive feedback, (**C**) negative feedback, (**D**) activator-repressor network with activator σ^{28} and repressor cl, and (**E**) activator-repressor network with activator σ^{38} and repressor cl. (**F**) Maximal GFP intensity as a function of the capillary length for the constructs in (A) to (C). Error bars represent standard variation over three repeats. Fluorescence images of (**G**) DNA brushes before expression and (**H**) GFP expression of the unregulated construct after 3 hours. Scale bar, 100 μm.

order, lighting up first in the short capillary (50 μm) and attaining low expression levels compared with longer capillaries (Fig. 2A and movie S1). The onset time, $\tau_{on}(L)$, was indeed linear in the capillary length for the three constructs, as predicted (fig. S7). In the positive-feedback construct, there was a long delay, 1 to 2.5 hours, before expression onset. The steady-state protein levels of the unregulated and positive-feedback constructs were proportional to τ and increased linearly with the capillary length over an order of magnitude (Fig. 2F), in accord with the solution to the diffusion equation (supplementary materials). The negative-feedback construct expression levels were low and independent of length for $L > 100$ μm (Fig. 2F). For short capillaries, $L < 100$ μm, steady state was not maintained because of rapid diffusion through the channel. All constructs showed a linear GFP profile along the capillary (fig. S8). Expression levels showed 10% variation between experiments (figs. S9 and S10).

We next explored the activator-repressor network, which exhibited oscillations and pulses of gene expression. In the first network (Fig. 2D), we used the sigma factor σ^{28} for activation and the cI repressor (as in Fig. 1E). The network exhibited oscillations with a period linear in the capillary length (fig. S11). Oscillations were also obtained at a different activator:repressor DNA stoichiometry and with the addition of a Cro
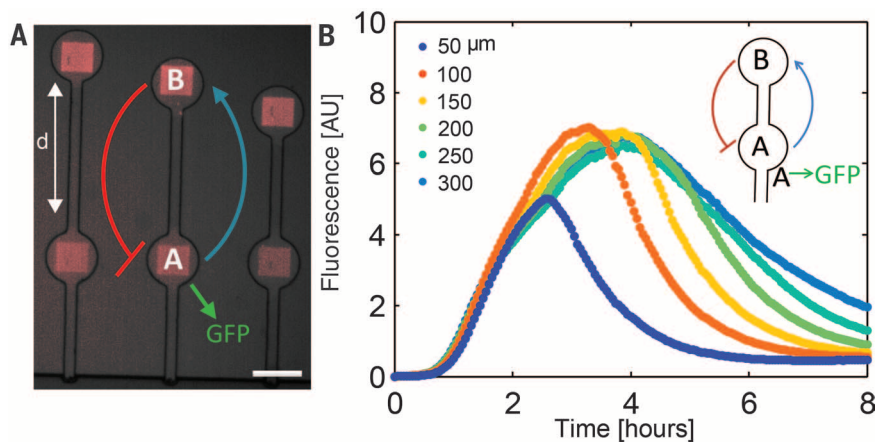
Fig. 3. Communication between DNA compartments. (**A**) Fluorescent image of DNA brush overlaid with the activator (denoted A)–repressor (denoted B) network scheme. The distance between compartments A and B varied, d = 50 to 300 μm. Scale bar, 100 μm. (**B**) GFP expression kinetics at compartment A for different distances between compartments, as denoted.
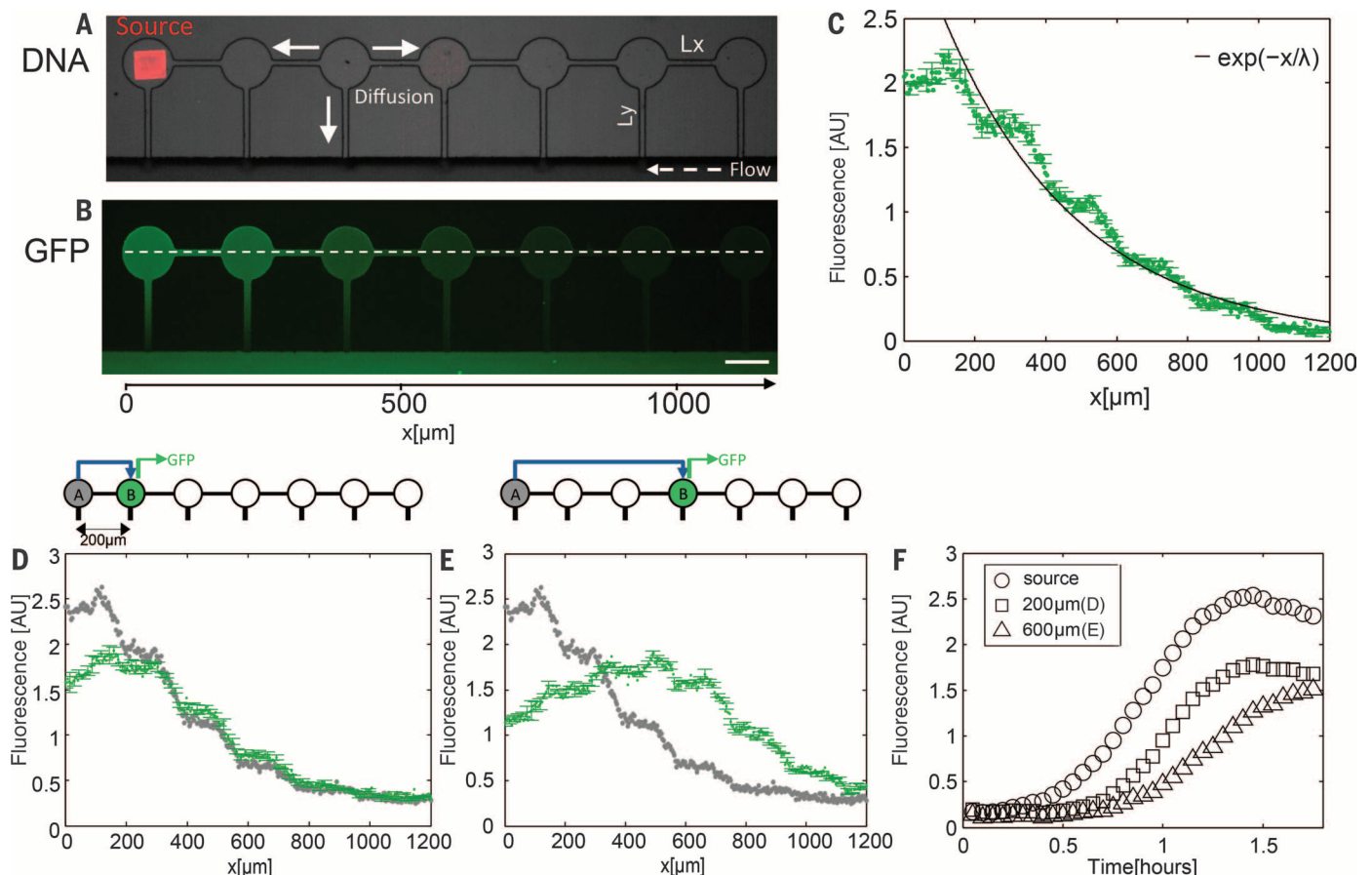
Fig. 4. Protein gradients in one-dimensional arrays. (**A**) DNA brush patterned in an array of seven connected compartments. (**B**) Image of GFP gradient after 3 hours of expression and (**C**) the resulting profile along the x axis. Solid line is an exponential fit, $e^{-x/\lambda}$, with λ = 380 ± 40 μm averaged over three experiments. Scale bar, 100 μm. (**D** to **F**) A one-step gene expression cascade in the array: activator (denoted A) patterned in the first compartment and activated GFP (denoted B) patterned at the (D) second or (E) fourth compartment. In green is the GFP profile expressed from gene B. In gray, the activator profile, as measured in a parallel array on the same chip. Error bars in (C) to (E) represent standard deviation of fluorescence data in a single gradient. (F) Kinetics of GFP expressed from gene A (circles) and gene B at the second (squares) and fourth (triangles) compartments.

repressor protein (fig. S11). By replacing the activator with a weaker sigma factor, σ^{38}, we obtained a single pulse dynamics (Fig. 2E). Increasing the ratio of activator to repressor genes in the brush changed the dynamics from a pulse to a steady state of high expression levels (fig. S12). Targeting degradation of GFP fused to SsrA or YbaQ tags by the ClpXP complex endogenously present in the cell-free extract (21) showed no detectable difference in dynamics (fig. S13).

We next showed diffusion-based communication with the activator-repressor network separated into two connected compartments (Fig. 3 and movie S2). Compartment A was positioned 200 μm away from the feeding channel, and the distance to compartment B varied, $d = 50$ to 300 μm. Compartment A was patterned with activator genes coding for the transcription initiation factor σ^{38} and a GFP reporter (Fig. 3A). Compartment B encoded for the lambda phage repressor cI regulated by a σ^{38} promoter. GFP appeared after 1 hour in compartment A for all capillary lengths and independently of d (Fig. 3B and fig. S14). After expression in compartment A, the activator σ^{38} diffused into compartment B and activated the cI repressor expression. In turn, the repressor diffused back to compartment A and shut down σ^{38} expression, thereby creating a spatiotemporal pulse (Fig. 3B). The typical time at which expression shuts off varied from 4 to 8 hours and was linear with d (fig. S14). In a related experiment, the positions of A and B were exchanged, resulting in a pulse with onset time and pulse width proportional to d (fig. S15).

A one-dimensional array of seven compartments was assembled parallel to the flow channel (Fig. 4). The compartments, $d = 200$ μm apart, were interconnected by capillaries of length $L_x = 100$ μm and connected to dilution capillaries of length $L_y = 150$ μm (Fig. 4A). A DNA brush coding for GFP was patterned in the first compartment of the array. A gradient of GFP appeared along the array with a maximum intensity at the DNA compartment, drop-

ping in a series of linear steps between neighboring compartments, and with a constant intensity within the compartments (Fig. 4, B and C). The overall profile had an exponentially decaying envelope, $e^{-x/\lambda}$, with a decay length $\lambda = 380 \pm 40$ μm averaged over three experiments. By considering the diffusion equation in the array, we theoretically derived a similar value, $\lambda = d\sqrt{\frac{L_y}{L_x}} = 245$ μm, that is determined only by geometry and is independent of protein diffusion constant (supplementary materials).

To examine the response to a signaling molecule in the one-dimensional array, we used a gene expression cascade. The activator gene, coding for σ^{28}, was patterned in the first compartment of the array and a GFP under a σ^{28} promoter in the second or fourth compartment (Fig. 4, D and E). The activator gene generated a protein concentration gradient along the array, and the reporter gene generated a profile that was maximal at the reporter compartment and decayed along the array in a piecewise linear profile. The reporter gene was activated with a delay that was dependent on its location along the array and distance from the source (Fig. 4F). The asymmetry in the GFP profile along the array (Fig. 4E) originated from residual flow between compartments (fig. S16).

The present approach for an artificial cell offers a means to program a variety of gene expression reactions and biological networks with a high degree of control that is amenable to prediction and theoretical modeling (22). The diffusion-based information transfer between adjacent compartments allows us to envisage a network of connected compartments with emergent spatial-temporal patterns as in morphogenesis.

REFERENCES AND NOTES

1. D. S. Tawfik, A. D. Griffiths, *Nat. Biotechnol.* **16**, 652–656 (1998).
2. V. Noireaux, A. Libchaber, *Proc. Natl. Acad. Sci. U.S.A.* **101**, 17669–17674 (2004).
3. V. Noireaux, R. Bar-Ziv, A. Libchaber, *Proc. Natl. Acad. Sci. U.S.A.* **100**, 12672–12677 (2003).
4. J. Kim, K. S. White, E. Winfree, *Mol. Syst. Biol.* **2**, 68 (2006).
5. E. Franco *et al.*, *Proc. Natl. Acad. Sci. U.S.A.* **108**, E784–E793 (2011).
6. A. J. Hockenberry, M. C. Jewett, *Curr. Opin. Chem. Biol.* **16**, 253–259 (2012).
7. M. Isalan, C. Lemerle, L. Serrano, *PLOS Biol.* **3**, e64 (2005).
8. D. Matthies *et al.*, *J. Mol. Biol.* **413**, 593–603 (2011).
9. Y. Heyman, A. Buxboim, S. G. Wolf, S. S. Daube, R. H. Bar-Ziv, *Nat. Nanotechnol.* **7**, 374–378 (2012).
10. J. Shin, P. Jardine, V. Noireaux, *ACS Synth. Biol.* **1**, 408–413 (2012).
11. A. S. Spirin, V. I. Baranov, L. A. Ryabova, S. Y. Ovodov, Y. B. Alakhov, *Science* **242**, 1162–1164 (1988).
12. T. Thorsen, S. J. Maerkl, S. R. Quake, *Science* **298**, 580–584 (2002).
13. D. Gerber, S. J. Maerkl, S. R. Quake, *Nat. Methods* **6**, 71–74 (2009).
14. H. Niederholtmeyer, V. Stepanova, S. J. Maerkl, *Proc. Natl. Acad. Sci. U.S.A.* **110**, 15985–15990 (2013).
15. P. Müller, K. W. Rogers, S. R. Yu, M. Brand, A. F. Schier, *Development* **140**, 1621–1638 (2013).
16. A. Buxboim *et al.*, *Small* **3**, 500–510 (2007).
17. D. Bracha, E. Karzbrun, S. S. Daube, R. H. Bar-Ziv, *Acc. Chem. Res.* **47**, 1912–1921 (2014).
18. J. Shin, V. Noireaux, *J. Biol. Eng.* **4**, 8 (2010).
19. J. Shin, V. Noireaux, *ACS Synth. Biol.* **1**, 29–41 (2012).
20. J. Stricker *et al.*, *Nature* **456**, 516–519 (2008).
21. J. Shin, V. Noireaux, *J. Biol. Eng.* **4**, 9 (2010).
22. L. H. Hartwell, J. J. Hopfield, S. Leibler, A. W. Murray, *Nature* **402** (suppl.), C47–C52 (1999).

SUPPLEMENTARY MATERIALS

www.sciencemag.org/content/345/6198/829/suppl/DC1
Materials and Methods
Supplementary Text
Figs. S1 to S16
Tables S1 to S3
References (23–27)
Movies S1 and S2